1 *Article*

2 Image Features Based on Characteristic Curves and
3 Local Binary Patterns for Automated HER2 Scoring

4 **Ramakrishnan Mukundan [1,*]**

5 [1] Department of Computer Science and Software Engineering, University of Canterbury, Christchurch,
6   New Zealand; mukundan@canterbury.ac.nz
7 * Correspondence: mukundan@canterbury.ac.nz; Tel.: +64-3-3692201

8

9   **Abstract:** This paper presents novel feature descriptors and classification algorithms for
10 automated scoring of HER2 in Whole Slide Images (WSI) of breast cancer histology slides.   Since a
11 large amount of processing is involved in analyzing WSI images, the primary design goal has been
12 to keep the computational complexity to the minimum possible level and to use simple, yet robust
13 feature descriptors that can provide accurate classification of the slides. We propose two types of
14 feature descriptors that encode important information about staining patterns and the percentage of
15 staining present in ImmunoHistoChemistry (IHC) stained slides. The first descriptor is called a
16 characteristic curve which is a smooth non-increasing curve that represents the variation of
17 percentage of staining with saturation levels. The second new descriptor introduced in this paper is
18 an LBP feature curve which is also a non-increasing smooth curve that represents the local texture of
19 the staining patterns. Both descriptors show excellent interclass variance and intraclass correlation,
20 and are suitable for the design of automatic HER2 classification algorithms.   This paper gives the
21 detailed theoretical aspects of the feature descriptors and also provides experimental results and
22 comparative analysis.

23   **Keywords:** medical image classification; local binary patterns; characteristic curves; whole slide
24   image processing; automated HER2 scoring

25
26

27 1. Introduction

28   The most commonly used method for breast cancer grading is the ImmunoHistoChemistry
29 (IHC) test which is a staining process performed on biopsy samples of breast cancer tissues [1]. The
30 IHC stained slides are normally observed under a microscope by pathologists to determine the level
31 of over-expression of Human Epidermal Growth factor Receptor 2 (HER2) protein in cancer cells.
32 The tissue sample is then assigned a HER2 score of 0 to 3+ representing the grade of cancer present
33 in the sample [2]. Manual grading and annotations of breast cancer slides are time consuming,
34 and there are huge maintenance costs associated with collecting, archiving, and transporting tissue
35 specimens. It is also well documented that manual grading can have significant variability in
36 pathologist assessments due to the subjective process of determining the intensity and uniformity of
37 staining in the presence of variable staining patterns and heterogeneity of tumor grade [3].
38 Automated methods can also suffer from errors due to inaccuracies in the training algorithm and its
39 inability to segment faint and complex tissue structures [4].
40   In the rapidly growing field of digital pathology, several Whole Slide Image (WSI) processing
41 algorithms are currently being developed as diagnostic tools to help pathologists in the assessment
42 of disease patterns [5]. WSIs have a pyramidal structure to enable optimized viewing across multiple
43 magnification levels, and they provide a high resolution overview of the entire slide [5,6]. Typically
44 at 40x magnification, the images have a resolution of approximately 0.25 microns per pixel. At this
45 resolution, a slide region of size 15mm x 15mm could correspond to 60,000 x 60,000 pixels. WSIs
46 were originally used as a computer aided digital microscopy tool, where pathologists could view
47 different parts of a sample at different magnifications to improve the accuracy of their scores [3].

48   Powerful computational algorithms are being developed to automatically extract features related to
49   cytological and protein structures in the image for accurately quantifying biomarkers like HER2 [7].
50   In [8], the authors used adaptive thresholding and watershed algorithm for cell segmentation.
51   Recently, an online contest was organized by the University of Warwick in conjunction with the
52   UK/Ireland Pathology Society annual meeting 2016, with the aim of advancing research in the field
53   of automated HER2 scoring algorithms [9]. This contest was the primary motivation for our research
54   work presented in this paper. Our algorithm (registered with team name UC-CSSE-CGIP)
55   performed exceedingly well in the contest, obtaining the second best points score of 390 out of 420
56   and the overall seventh position in the combined leader board [10]. The teams that were on the top of
57   the leader board, including our team, were invited to submit a very brief (one paragraph) summary
58   of the algorithms used for inclusion in a journal paper prepared by the contest organizers [11].

59   WSIs contain voluminous amounts of data. One of the primary design goals has been to keep
60   the computational complexity to the minimum possible level and to develop an efficient method that
61   can process relevant tiles of an input WSI image quickly and classify the image into one of the four
62   classes corresponding to the four HER2 scores. The second design goal was to have a feature set
63   whose correlation to the percentage of membrane staining in the given sample could be easily
64   visualized and interpreted by pathologists. The third design goal was to reduce the amount of
65   information redundancy in the feature set by extracting a minimal set of characteristic features that
66   would adequately represent the staining pattern and the percentage of staining. This paper presents
67   two types of feature descriptors that have shown excellent intraclass correlation and interclass
68   variance in our experimental analysis involving a large collection of WSI images. The first descriptor
69   is called characteristic curves and they represent the variation of the percentage of staining in an
70   image tile with saturation levels of the staining colour. The second descriptor is based on local
71   binary patterns [12], and they encode information about the local texture variation in the image with
72   saturation levels. The paper provides a detailed description of the WSI processing stages,
73   development and selection of features, and the experimental analysis performed. We hope that the
74   methods presented in this paper will contribute significantly to the development of faster and
75   accurate automatic HER2 scoring techniques in the area of breast cancer histopathology.

76   The paper is organized as follows: The next section gives a description of the dataset used, an
77   outline of HER2 assessment scheme and an overview of the stages of the processing pipeline.
78   Section 3 provides an introduction to a novel set of features called characteristic curves and
79   discusses their computational aspects and properties. Section 4 gives an overview of local binary
80   patterns, their computation, and introduces another set of feature descriptors called LBP feature
81   curves. Section 5 gives a brief description of a classification algorithm using the proposed feature
82   descriptors for classifying histopathological images based on their HER2 scores. and Section 5
83   presents experimental results and comparative analysis. Section 6 presents experimental results
84   and analysis. Section 7 concludes the paper with a summary of important aspects of the proposed
85   features and outlines future research directions.

86   **2. Materials and Methods**

87   *2.1 HER2 Assessment*

88   The amplification of HER2 genes and correspondingly the over-expression of HER2 protein
89   receptors play an important role in the development of breast cancer. The assessment of HER2
90   protein over-expression is done using the ImmunoHistoChemistry (IHC) test based on the
91   percentage of membrane staining observed in tumor cells as well as the intensity of staining [2]. The
92   mapping between the level of membrane staining and the reported HER2 score is shown in Table 1.
93

94
95

Table 1. Correlation between the intensity and percentage of membrane staining and the assigned HER2 scores [2].

HER2 Score	Assessment	Staining Pattern
0	Negative	No staining is observed, or membrane staining is observed in less than 10% of tumor cells
1+	Negative	A faint/barely perceptible membrane staining is detected in greater than 10% of tumor cells. The cells exhibit incomplete membrane staining.
2+	Weakly Positive	A weak to moderate membrane staining is observed in greater than 10% of tumor cells.
3+	Positive	A strong complete membrane staining is observed in greater than 10% of tumor cells.

96
97
98
99
100

A few sample tiles from WSI images of IHC stained slides are given in Figure. 1 along with the HER2 scores to show the variations of the scores with the level of membrane staining seen in the images.
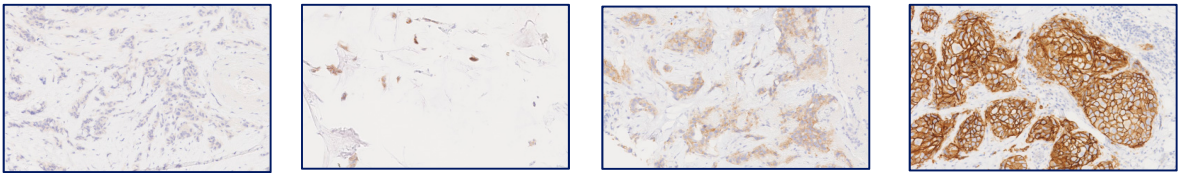
HER2 Score = 0   HER2 Score = 1+   HER2 Score = 2+   HER2 Score = 3+

101   **Figure 1.**   WSI tiles showing different levels of staining and corresponding HER2 scores.

102   *2.2 Dataset*

103
104
105
106
107
108
109
110

The dataset used in this research work was provided by the University of Warwick as part of the online HER2 scoring contest [9]. Permission was granted by the contest organizers to participating teams for the use of the dataset for research and academic purposes. The dataset consisted of a total of 172 whole slide images in Nano-zoomer Digital Pathology (NDPI) format. These WSIs were extracted from 86 cases of patients with invasive breast carcinomas [11].   For each case, WSIs of both Hematoxylin and Eosin (H&E) stained and IHC stained slides were provided. There were two HER2 scoring contests, and the number of WSIs provided for training and testing the classification algorithm is given in Table 2.

111   **Table 2.** Number of WSIs provided for training and testing the classification algorithm.

Training Set		Test Set	
Ground Truth HER2 Score	Number of WSIs	Contest-1 No. of WSIs	Contest-2 No. of WSIs
0	13	**28**	**6**
1+	13		
2+	13		
3+	13		
Total:	**52**		

112

113   *2.3 Processing Stages*

114
115

Various stages of the processing pipeline are shown in Figure 2. We used the OpenSlide API [13] to read WSIs of IHC stained slides, and a region of interest (ROI) containing a significant portion

116   of the imaged tissue is extracted   from the middle segment of the image.   Rectangular tiles of size
117   1800 x 1200 pixels at 20x magnificaiton that contain at most 20% background pixels are then created
118   and used as inputs for the method that computes LBP features and characteristic curves.   At least
119   six tiles at randomly selected locations within the ROI are generated for each WSI. The remaining
120   part of the pipeline thresholds the input tiles and computes the LBP features and also the percentage
121   of staining in the tissue sample to obtain the characteristic curves. These steps are detailed in the
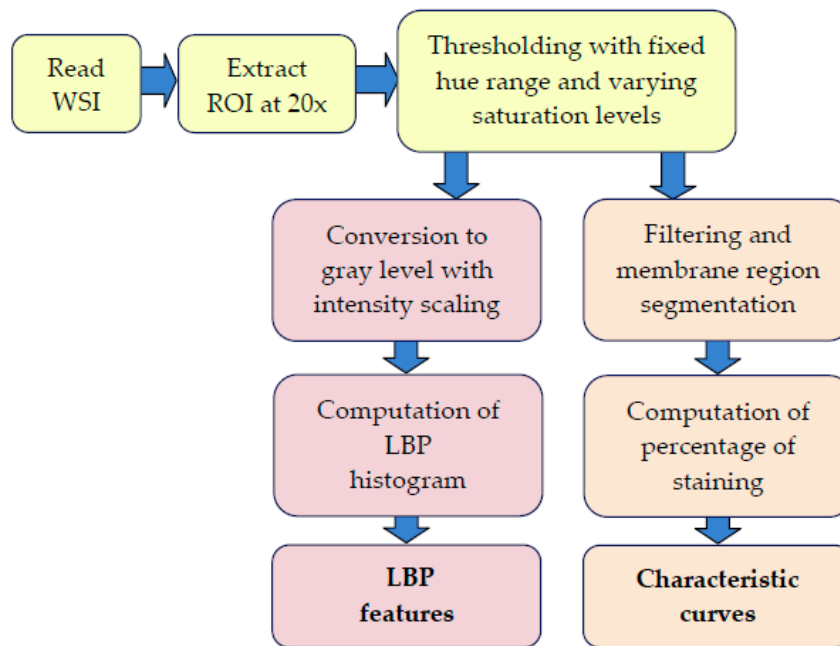122   following sections.
123

124
125   **Figure 2.** Processing stages in the extraction of characteristic curves and LBP features

126   **3. Characteristic Curves**

127   Curve based automated analysis of immunohistochemical images have been tried in the past
128   with limited success [14]. In this section, we introduce a novel feature vector called a characteristic
129   curve. An important parameter in HER2 assessment is the percentage of membrane staining
130   perceived in an image segment. Assuming that we can compute the percentage of membranes
131   stained in a particular colour range (this computation will be discussed in detail below), we can
132   analyse the variations in this percentage value with respect to changes in the colour saturation
133   threshold.   Specifically, if [h, s, v] represent the stain colour components in HSV space, and if $p(s_{low})$
134   denotes the pecentage of staining with colour in the range given by the following inequalities:

$$h_1 \leq \ h \ < \ h_2$$

$$s > s_{low}$$

$$v_1 \leq \ v \ < \ v_2, \tag{1}$$

135   then, the variation of $p(s_{low})$ plotted against s_{low} gives the characteristic curve (or the
136   percentage-saturation curve) of the image. In Equation 1, [h_1, h_2] denote fixed hue thresholds
137   specifying allowable variations in the hue value, and similarly [v_1, v_2] denote value thresholds.
138   Since we specify only the lower bound for saturation, progressively increasing s_{low}, typically from 0.1
139   to 0.5, produces a non-increasing characteristic curve (Figure 3).
140   The base components of the stain colour [h, s, v] are computed using the training set where the
141   given percentage of staining is above 80%.   While computing the percentage of staining for the test
142   (or cross-validation) sets, it is important to eliminate not only the background region but also other
143   segments that are not part of the membrane region such as connective tissues, lobules and nuclei.

144 These regions can be segmented using colour (nuclei are stained in a distinctly different colour) or
145 using a distance measure evaluated in colour space over a neighborhood mask around each pixel
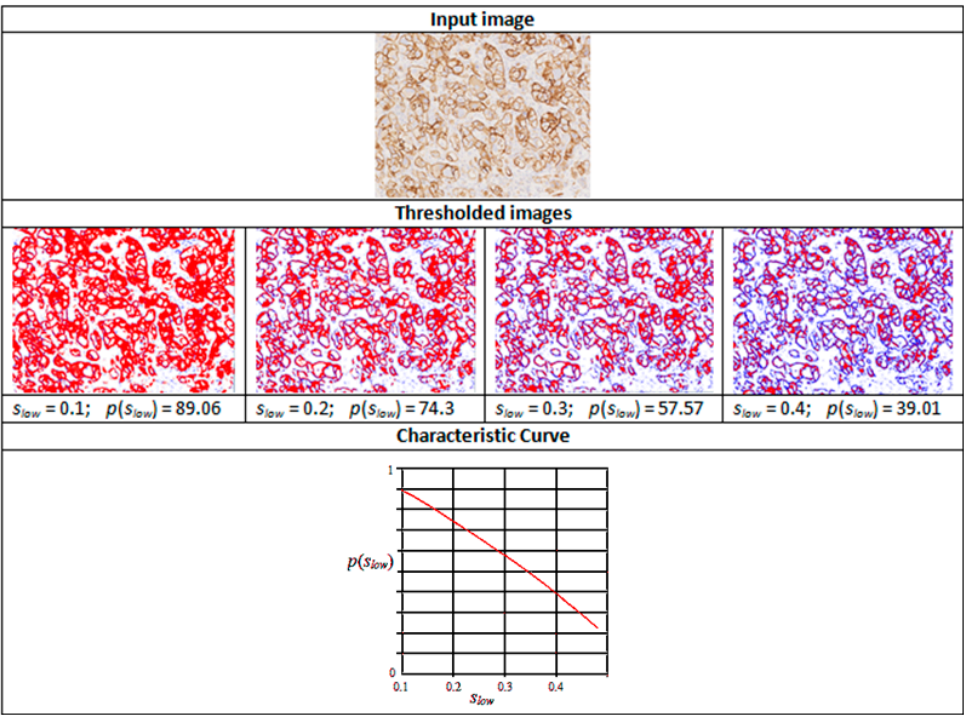146 (for identifying regions of nearly constant colour value)
147

148
149   **Figure 3.** Intermediate stages in the generation of a characteristic curve.

150   Figure 3 shows thresholded images with stained regions in red colour as the value of s_{low} is
151 increased from 0.1 to 0.4. The resulting characteristic curve is also shown. The characteristics curves
152 have the property that they are always monotonically decreasing smooth curves. They allow
153 accurate polynomial approximations using cubic curves. The shape of the curve can be directly
154 matched with the staining patterns given in the HER2 assessment guidelines (Table 1) for a
155 straightforward interpretation of the derived score (Figure 4). For example, the characteristic curve
156 always lies below the 10% threshold when the score is 0, and only a small initial segment of the curve
157 lies above the 10% mark when the score is 1. If the score is 3+, the curve lies completely above the
158 30% mark showing a strong and complete membrane staining. As seen in Figure 4, the curve passes
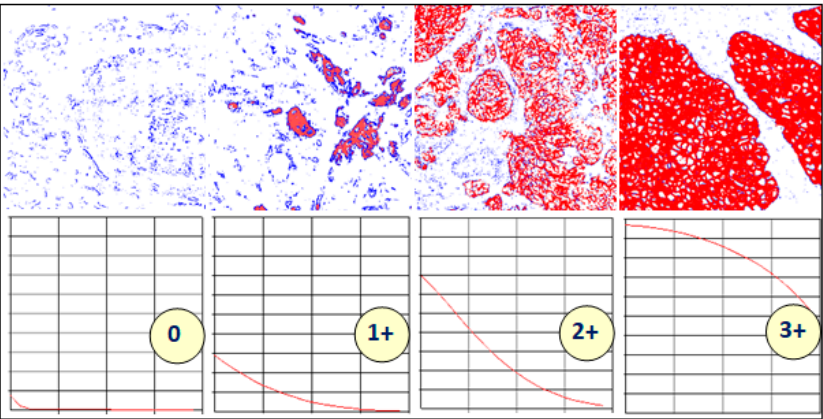159 through a much wider range of values of percentage staining when the score is 2+.
160

161
162   **Figure 4.** Variations in the shapes of the characteristic curves with different levels of staining.

163   The properties of the characteristic curve outlined above, particularly the fact that the curve is
164   non-increasing, can be used for developing a naive rule-based classification algorithm as follows.
165   • If z_0 ($= p(0.1)$) < 10%, then the whole curve lies below 10%, and the score is 0
166   • Else if z_{n-1} ($= p(0.5)$) > 30%, then the whole curve lies above 30%, and the score is 3+
167   • Else if 10% ≤ z_0 ($= p(0.1)$) < 40% and $p(0.2)$ < 15%, the score is 1+
168   • Else if $p(0.4) < 15\%$, then the score is 2+
169   • Else, the score is 3+
170   The rules were formed by analyzing the shapes of characteristic curves for several image tiles
171   with ground truth values of HER2 scores assigned by pathologists. Note that for the above simple
172   classification algorithm, we sample the curve at only four key points $p(0.1)$, $p(0.2)$, $p(0.4)$, and
173    $p(0.5)$. We outlined the rule based algorithm here primarily to show the feature representation
174   capability of the characteristic curves.

175   **4. Local Binary Patterns**

176   *4.1 LBP Computation*

177   Local binary patterns (LBP) are powerful feature descriptors used for texture analysis and
178   classification [12]. The binary pattern is derived by comparing the intensity at each pixel with its
179   eight neighbors and encoding the information in an 8-bit integer value. This encoding can be viewed
180   as a transformation of the input image into an LBP image as shown in Figure 9. The histogram of the
181   LBP image is generally used for texture classification. In the area of medical image analysis, LBP
182   methods have been successfully used in characterizing disease patterns [15-17] and automated
183   diagnosis [18]. Local binary patterns have also been used for analyzing histopathological images and
184   detecting mitotic cells [19,20]. Several variants of LBP features such as hierarchical LPB have also
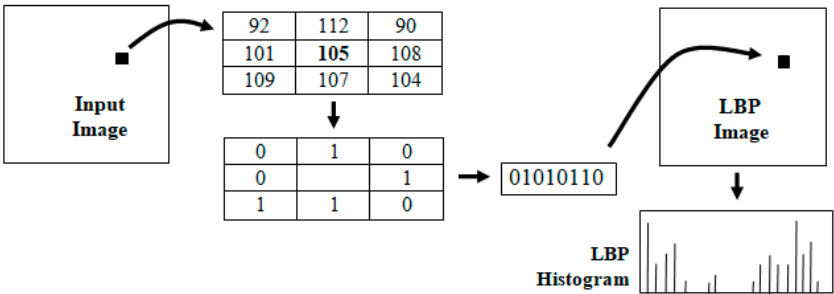185   been proposed for specific applications like retinal vein occlusion recognition [21].
186

187
188   **Figure 5.** The intermediate steps in the computation of the LBP histogram of an image.

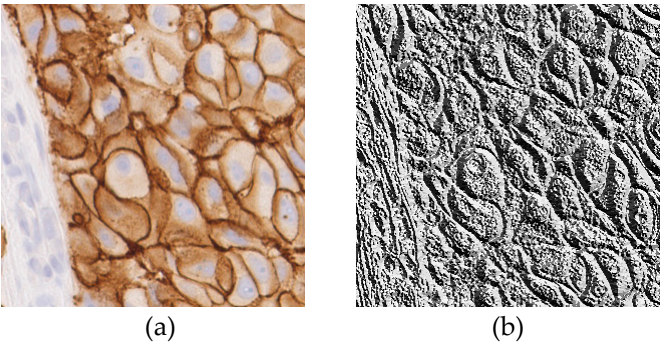189   As an example, an input image and its LBP image are shown in Figure 6.
190

(a)   (b)

191   **Figure 6.** (**a**) A sample input image for LBP computation; (**b**) The corresponding LBP image.

192

193   As discussed in Section 3, we first obtain a thresholded image using a hue range $[h_1, h_2]$ and
194   saturation values with $s > s_{low}$.   The pixels passing the threshold test are converted to gray level by
195   mapping h_1 to 0 and h_2 to 255. This gray level image is used as the input for LBP computation. The
196   LBP histogram of such images contain predominant features that represent the texture characteris-
197   tics of the staining patterns.

198   *4.2 LBP Feature Curves*

199   An LBP histogram is shown in Figure 7. The important LBP features are highlighted based on
200   their magnitudes. The LBP histogram contains 256 values L_i , $i = 0...255$.   We propose the fol-
201   lowing set of five LBP features for classification:

202                      $V = \{L_2, L_{32}, L_{128}, L_{223}, L_{253}\}$ (2)
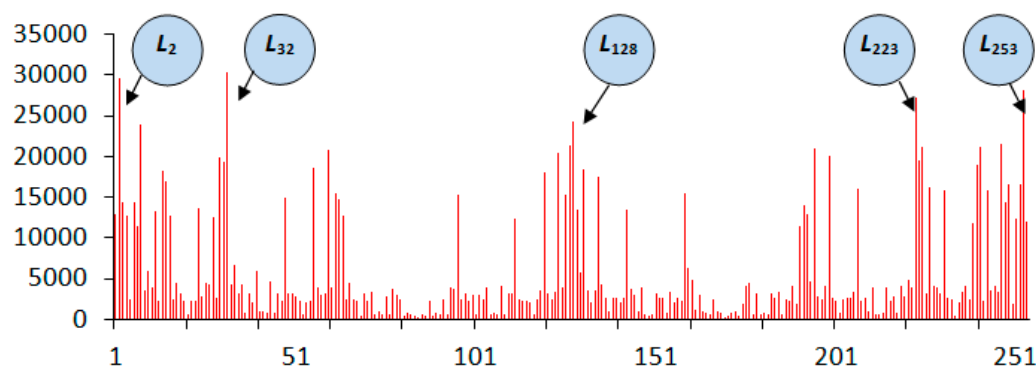
203

204

205   **Figure 7.** An LBP histogram showing the predominant feature components.

206   Each feature in the above set can generate a feature curve as detailed below. Consider one of the
207   LBP feature components, say L_{32}. When the input image's saturation threshold s_{low} is varied from 0.1
208   to 0.4 as discussed in Section 3, we get the corresponding variation in L_{32}. This variation in the values
209   of L_{32} shows a non-increasing trend very similar to that of the characteristic curve.

210

211

212   **Figure 8.** Normalized LBP feature curves for L_{32}, L_{128}, L_{253} showing the variations of their magnitudes
213   when the values of the saturation threshold s_{low} are varied from 0.1 to 0.8 (*x*-axis).

214   The values of the LBP feature curves are normalized to remove any variations due to changes in
215   image size as follows:

                           $L_i' = L_i.100/(w.h)$ (2)

216 where, w, h denote the width and the height of the input image. The variations of three LBP
217 feature components L'_{32}, L'_{128}, and L'_{253} with the saturation threshold for images with HER2 scores 0,
218 1+, 2+ and 3+ are shown in Figure 8.
219 The LBP feature curves bear similarity with characteristic curves in that they do not contain
220 high frequency variations and are non-increasing. Further, as can be seen in Figure 8, LBP feature
221 curves also show excellent discriminating power between the four HER2 classes, making them
222 suitable for use as feature vectors in classification algorithms.

223 5. HER2 Classification and Scoring

224 In this section, we outline a 'one-vs-all' multi-class classification algorithm using logistic re-
225 gression [22]. Logistic regression was chosen to minimize the computational complexity. Higher
226 order methods such as neural networks could also be designed with the use of the feature vectors
227 proposed in this paper. For a given training example with index j, the points sampled along its
228 characteristic curve or LBP feature curve $x_i^{(j)} = p(s_i)$, $i = 1..n$, $j = 1..m$ are used as features. The class
229 labels are denoted by $y_j \in [0, 3]$, $j = 1..m$. We denote the feature matrix by $X \in \Re^{m \times (n+1)}$, the output
230 vector of labels by $Y \in \Re^{m \times 1}$, and the classifier parameter vector for each class by $\theta_k \in \Re^{(n+1) \times 1}$, $k = 1..4$.
231 Here, class-1 corresponds to the set of training examples with HER2 score 1+, class-2 with HER2
232 score 2+, class-3 with HER2 score 3+ and class-4 with HER2 score 0. We then have the following
233 equations for the hypothesis functions H, the cost function and the gradient functions:

$$H = g(X\theta_k) \tag{3}$$

234 where, $H \in \Re^{m \times 1}$, and $g()$ denotes the sigmoid function. The cost function $J(\theta_k)$ is then given by

$$J(\theta_k) = -\frac{1}{m}\left(Y^T \log(H) - (1-Y)^T \log(1-H)\right) \tag{4}$$

235 and the gradient function vector $J'(\theta_k)$ is defined as

$$J'_k(\theta) = -\frac{1}{m}\left(X^T(H-Y)\right), \quad k = 1..4. \tag{5}$$

236 For prediction, the points x_i on the characteristic curve or the LBP feature curve of a given
237 sample are combined with the trained values of class parameters θ_k for each class $k = 1..4$, and the
238 class that gives the maximum value for $g(x_i'\theta_k)$ is chosen. In the next section, we provide the result
239 of classification experiments using the above methods.

240 6. Experimental Results and Analysis

241 We used features computed from 52 WSIs with 3 tiles at 20x from each image (comprising of
242 156 images) and their ground truth values as the training data. Another set of 3 tiles from each of the
243 52 cases formed the cross-validation set. Out of the total of 156 image tiles in the cross-validation
244 set, 39 belonged to each of the four classes corresponding to four HER2 scores. For generating fea-
245 ture vectors for classification using logistic regression, it was found that a step size of 0.02 for the
246 saturation threshold would provide an adequate number of 20 points (features) within the satura-
247 tion range $s_{low} \in [0.1, 0.5]$. The feature matrix X in Equation 3 therefore had the dimension 156×20.
248 The gradient descent algorithm used 100 iterations to converge to the solution with a learning rate of
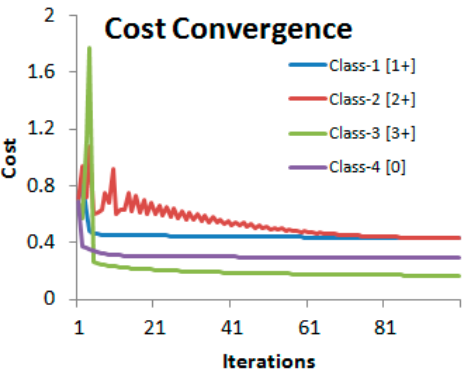249 0.001 (Figure 9).

Figure 9. Convergence of the cost functions of the four-class logistic regression algorithm.

Figure 9 gives a sample plot of cost function values for each of the four classes, where the characteristic curves consisting of 20 features for each sample were used as feature vectors. The confusion matrix in Table 3 summarizes the results for each class and gives the overall accuracy achieved.

Table 3. Confusion matrix for the multi-class logistic regression algorithm

		Predicted				Accuracy = 88.46%	
		0	**1+**	**2+**	**3+**	**Precision**	**Recall**
Actual	**0**	37	2	0	0	0.86	0.95
	1+	6	29	4	0	0.83	0.74
	2+	0	4	34	1	0.87	0.87
	3+	0	0	1	38	0.97	0.97

The smoothness and monotonically decreasing properties of the characteristic curve can be effectively made use of in reducing the dimensionality of the features in the logistic regression algorithm. As in the case of the rule based classification method, we can sample the curve at only four key points $p(0.1)$, $p(0.2)$, $p(0.4)$, and $p(0.5)$, and also use the slope information at those points $p'(0.1)$, $p'(0.2)$, $p'(0.4)$, and $p'(0.5)$ to get a feature vector of size 8 instead of 20. The cost functions converge to almost similar values with only a slight increase in the magnitudes. The confusion matrix obtained by running the algorithm with the reduced set of features of the characteristic curve is shown in Table 4.

Table 4. Confusion matrix for the multi-class logistic regression algorithm with the reduced feature set.

		Predicted				Accuracy = 83.3%	
		0	**1+**	**2+**	**3+**	**Precision**	**Recall**
Actual	**0**	37	2	0	0	0.80	0.95
	1+	8	24	7	0	0.75	0.61
	2+	1	6	31	1	0.79	0.79
	3+	0	0	1	38	0.97	0.97

As seen in Table 4, reducing the dimensionality of the feature set from 20 to 8 only affected the recall rates of classes 1 and 2.

Experimental analysis using LBP feature curves also gave reasonably good levels of accuracy. Only one LBP feature curve selected from the set in Equation 2 was used in our analysis, and the feature vector consisted of 20 sample points along the curve. We give below the results for the feature curve L_{32} (Table 5).

275 **Table 5.** Confusion matrix for the multi-class logistic regression algorithm with the LBP feature
276 vector L_{32}.

		Predicted				Accuracy = 87.18%	
		0	**1+**	**2+**	**3+**	**Precision**	**Recall**
Actual	**0**	38	1	0	0	0.84	0.97
	1+	6	27	6	0	0.82	0.69
	2+	1	5	32	1	0.84	0.82
	3+	0	0	0	39	0.98	1.00

277
278
279 The texture characteristics represented by LBP features were useful in resolving some of the
280 ambiguous cases for scores 0 and 3+ where the texture features are highly distinguishable, providing
281 higher recall rates for those two scores. The LBP features also gave higher false positives for score 2+.
282 Overall, logistic regression with 20 feature points computed from the characteristic curves gave the
283 highest accuracy of 88.5%.
284 Analysing the staining patterns in tiles that were wrongly classified revealed a common prob-
285 lem in the automatic extraction of tiles from WSIs. Some of the samples with scores 1+ and 2+ had
286 large tissue regions without any staining. The example shown in Figure 10 contains a tissue sam-
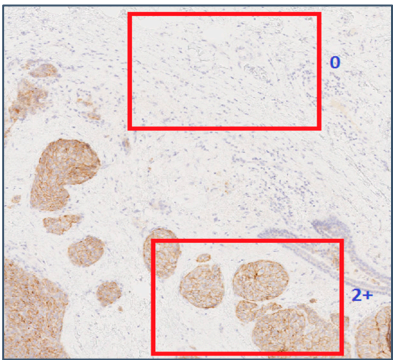287 ple at 10x magnification with an assigned score of 2+.
288

289
290 **Figure 10.** An example showing two tile positions with varying image characteristics within the same
291 WSI.

292 In Figure 10, the tile on the top did not contain any stained membrane regions and was assigned
293 a ground truth value of 2+ at the training stage, and a predicted value of 0 at the cross-validation
294 stage. This tile could have been a valid part of any WSI with a score 0, and therefore there is no way
295 by which such tiles can be identified and discarded by the automatic tile extraction method.
296 Manually identifying such tiles from the training and cross-validation sets significantly improved
297 the scores of the classification algorithms. The tile on the bottom half of Figure 10 was assigned the
298 correct score of 2+.

299 **7. Conclusions and future work**

300 This paper has introduced two novel feature descriptors *viz.*, characteristic curves and LBP
301 feature curves that could be effectively used in classification algorithms for automated scoring of
302 HER2 in breast cancer histology slides. The computational aspects of both types of descriptors and
303 their shape feature representation capabilities in embedding information about the staining patterns
304 and the percentage of staining present in images with different HER2 scores have been discussed in
305 detail. Both descriptors have similar geometrical attributes in that they are both smooth
306 non-increasing curves. Experimental analysis have shown that both descriptors have excellent in-

307 terclass variance and intraclass correlation properties that make them useful for applications in
308 classification algorithms. Results of experimental analysis done using a comprehensive WSI dataset
309 provided by the University of Warwick[9] has also been presented. The results show that the fea-
310 tures used with a multi-class classification algorithm such as logistic regression can provide very
311 good levels of accuracy. The paper also outlined computational stages in the overall processing
312 pipeline for automatic HER2 scoring using WSI files as inputs.

313   Experimental results given in the paper also show the need for further improving the discrim-
314 inating power of the features. Future work is directed towards performing detailed feature analysis
315 to select a combination of features from characteristic curves and LBP feature curves. Further
316 analysis is required for accurate identification of membrane morphology and region segmentation,
317 particularly for samples with an assigned HER2 score 1+. It is also necessary to assess the repro-
318 ducibility of results, specifically inter-scanner variability [23] of the rule-based classification algo-
319 rithm as the rules were formed using data produced by a single scanner. Future work is also directed
320 towards GPU implementations of the feature extraction methods.

References

321 **References**

322 1. Hicks, D.G.; Schiffhauer, L. Standardized assessment of the HER2 status in breast cancer by
323   immunohistochemistry. *Lab. Med.* **2015**, 42(8), 459-467, DOI: 10.1309/LMGZZ58CTS0DBGTW
324 2. Rakha, E.A., et.al. Updated UK recommendations for HER2 assessment in breast cancer. *J. Clin. Pathol.*
325   **2015**, 68, 93-99, DOI: 10.1136/jclinpath-2014-202571
326 3. Gavrielides, M.A.; Gallas, B.D.; Lenz, P.; Badano, A.; Hewitt, S.M. Observer variability in the
327   interpretation of HER2 immunohistochemical expression with unaided and computer aided digital
328   microscopy. *Arch Pathol Lab Med*. **2011**, 135(2), 233-242, DOI: 10.1043/1543-2165-135.2.233
329 4. Akbar, S.; Jordan, L.B.; Purdie, C.A.; Thompson, A.M.; McKenna, S.J. Comparing computer-generated
330   and pathologist-generated tumour segmentations for immunohistochemical scoring of breast tissue
331   microarrays. *Br J Cancer* **2015**, 113(7), 1075-1080, DOI: 10.1038/bjc.2015.309
332 5. Hamilton, P.W., et.al. Digital pathology and image analysis in tissue biomarker research. *Methods* **2014**,
333   70(1), 59-73, DOI: 10.1016/j.ymeth.2014.06.015
334 6. Farahani, N.; Parwani, A.V.; Pantanowitz, L. Whole slide imaging in pathology: advantages, limitations
335   and emerging perspectives. *Path. Lab. Med. Intl*. **2015**, 7, 23-33, DOI: 10.2147/PLMI.S59826
336 7. Ghaznavi, F.; Evan, A.; Madabhushi, A.; Feldman, M. Digital imaging in pathology: Whole-slide imaging
337   and beyond. *Annul. Rev. Pathol. Mech. Dis*. **2013**, 8, 31-59, DOI: 10.1146/annurev-pathol-011811-120902
338 8. Razavi, S.; Hatipoglu, G.; Yalcin, H. Automatically diagnosing HER2 amplification status for breast cancer
339   patients using large FISH images. Proceedings of 25th Signal Processing and Communications
340   Applications Conference, Antalya, Turkey, 15-18 May 2017, 1-4, DOI: 10.1109/SIU.2017.7960428
341 9. Department of Computer Science, University of Warwick: Her2 Scoring Contest. Available online:
342   http://www2.warwick.ac.uk/fac/sci/dcs/research/combi/research/bic/her2contest/ (accessed on 15 Nov
343   2016).
344 10. Department of Computer Science, University of Warwick: Her2 Contest Results. Available online:
345   http://www2.warwick.ac.uk/fac/sci/dcs/research/combi/research/bic/her2contest/outcome (accessed on 15
346   Nov 2016).
347 11. Qaiser, T., et.al. HER2 Challenge Contest: A detailed assessment of HER2 scoring algorithms and man vs
348   machine in whole slide images of breast cancer tissues. *Histopathology* **2017**. DOI: 10.1111/his.13333
349 12. Pietikainen, M.; Zhao, G.; Hadid, A.; Ahonen, T. *Computer Vision Using Local Binary Patterns*,
350   Springer-Verlag, London, ISBN: 978-0-85729-748-8.
351 13. Goode, A.; Gilbert, B.; Harkes, J.; Jukie, D.; Satyanarayanan, M. OpenSlide: A vendor-neutral software
352   foundation for digital pathology. *J. Pathol. Inform*. **2013**, 4(27), DOI: 10.4103/2153-3539.119005.
353 14. Livanos, G.; Zervakis, M.; Giakos, G.C. Automated analysis of immunohistochemical images based on
354   curve evolution approaches. Proceedings of IEEE conference of Imaging Systems and Techniques, Beijing,
355   China, 22-23 Oct 2013, 112-115, DOI: 10.1109/IST.2013.6729673
356 15. Sørensen, L.; Shaker, S.B.; Bruijne, M. de. Quantitative analysis of pulmonary emphysema using local
357   binary patterns, *IEEE Transactions on Medical Imaging* **2010**, 29(2), 559-569, DOI: 10.1109/TMI.2009.2038575.

16. Morales, S.; Engan, K.; Naranjo, V.; Colomer, A. Detection of diabetic retinopathy and age-related macular degeneration from fundus images through local binary patterns and random forests, Proceedings of IEEE International Conference on Image Processing, Quebec, Canada, 27-30 Sep 2015, 4838-4842, DOI: 10.1109/ICIP.2015.7351726

17. Sarwinda, D.; Bustamam, A. Detection of Alzheimer's disease using advanced local binary pattern from hippocampus and whole brain of MR images, Proceedings of International Joint Conference on Neural Networks, Vancouver, Canada, 24-29 July 2016, 5051-5056, DOI: 10.1109/IJCNN.2016.7727865

18. Tiwari, A.K.; Pachori, R.B.; Kanhangad, V.; Panigrahi, B.K. Automated diagnosis of epilepsy using key-point based local binary pattern of EEG signals, *IEEE Jnl. Biomed. Health Info.* **2017**, 21(4), 888-896, DOI: 10.1109/JBHI.2016.2589971

19. Urdal, J.; Engan, K.; Kvikstad, V.; Janssen, E.A.M. Prognostic prediction of histopathological images by local binary patterns and RUSBoost, Proceedings of the 25th European Signal Processing Conference, Kos, Greece, 2 Sep 2017, 2349-2353, DOI: 10.23919/EUSIPCO.2017.8081630

20. Sigirci, I.O.; Albayrak, A.; Bilgin, G. Detection of mitotic cells using completed local binary pattern in histopathological images, Proceedings of 23rd Signal Processing and Communications Applications Conference, Malatya, Turkey, 16-19 May 2015, 1078-1081, DOI: 10.1109/SIU.2015.7130020

21. Zhang, H.; Chen, Z.; Chi, Z.; Fu, H. Hierarchical local binary pattern for branch retinal vein occlusion recognition with fluorescein angiography images, *Electronics Lett.* **2014**, 50(25), 1902-1904, DOI: 10.1049/el.2014.2854

22. Watt, J.; Borhani, R.; Katsaggelos, A.K. *Machine Learning Refined: Foundations, Algorithms and Applications.*, 1st ed.; Cambridge Uni. Press: Cambridge, UK, 2016; ISBN: 978-1107123526.

23. Keay, T., et al. Reproducibility in the automated quantitative assessment of HER2/neu for breast cancer. *J. Pathol Inform.* **2013**, 4(19), DOI: 10.4103/2153-3539.115879.